





A spherical wave expansion for a steerable parametric array loudspeaker using Zernike polynomials

Jiaxin Zhong,¹  Ray Kirby,¹  Mahmoud Karimi,¹  and Haishan Zou^{2,a)} 

¹Centre for Audio, Acoustics and Vibration, University of Technology Sydney, New South Wales 2007, Australia

²Key Laboratory of Modern Acoustics and Institute of Acoustics, Nanjing University, Nanjing 210093, China

ABSTRACT:

A steerable parametric array loudspeaker (PAL) can electronically steer highly directional audio beams in the desired direction. The challenge of modelling a steerable PAL is to obtain the audio sound pressure in both near and far fields with a low computational load. To address this issue, an extension of the spherical wave expansion is proposed in this paper. The steerable velocity profile on the radiation surface is expanded as Zernike polynomials which are an orthogonal and form a complete set over a unit circle. An expression for the radiated audio sound is then obtained using a superposition of Zernike modes. Compared to the existing methods, the proposed expansion is computationally efficient and provides a rigorous transformation of the quasilinear solution of the Westervelt equation without paraxial approximations. The proposed expansion is further extended to accommodate local effects by using an algebraic correction to the Westervelt equation. Numerical results for steering single and dual beams are presented and discussed. It is shown that the single beam can be steered in the desired direction in both near and far fields. However, dual beams cannot be well separated in the near field, which cannot be predicted by the existing far field models. © 2022 Acoustical Society of America. <https://doi.org/10.1121/10.0014832>

(Received 26 June 2022; revised 19 September 2022; accepted 26 September 2022; published online 24 October 2022)

[Editor: Nickolas Vlahopoulos]

Pages: 2296–2308

I. INTRODUCTION

Parametric array loudspeakers (PALs) have been widely used in many audio applications due to their ability to generate highly directional sound beams.¹ PALs can also make use of the phased array technique to steer the audio beams,² which has the advantage of delivering narrow audio beams in the desired direction without the need to mechanically rotate the sound source. Steerable PALs have been investigated for applications such as active noise control and sound reproduction systems.^{3,4} In recent years, progress has been made in the signal preprocessing techniques and multi-beam design methods.^{4,5} However, the existing prediction methods are either limited to far-field calculations or very time-consuming for near-field predictions.^{6,7} This paper aims to develop a theoretical model for predicting audio sound generated by a steerable PAL that is accurate in the near field as well as computationally efficient.

When a PAL generates two intensive ultrasonic beams at two difference frequencies, the audio sound at the difference frequency is demodulated due to the nonlinear interaction between the beams.¹ For a steerable PAL, a velocity profile is assigned to the radiating surface of the PAL so that the audio beam can be steered in a desired direction. Theoretical models for steerable PALs normally focus on calculating the far field directivity of the audio sound. For example, early studies adopted the product directivity model, which determines the directivity of the audio sound

by the product of the ultrasonic directivities at two frequencies.² By approximating the directivity of ultrasonic transducer array using an equivalent circular Gaussian source array, Shi and Gan improved the prediction accuracy for the sidelobes of the product directivity model.⁸ Although the locations of the main, grating, and side lobes can be predicted using this model, the amplitude of these lobes was found to be inaccurate. A convolution model was then proposed to improve the accuracy, which calculates the directivity of the audio sound by calculating the convolution of the product of the directivity of the ultrasound and the Westervelt's directivity.^{6,9,10} However, differences between prediction and measurement continue to be observed.⁶ This is because the far field is more than 10 m away from a PAL when its diameter is larger than 0.04 m, while the measurement distance is usually within several meters.⁷ Therefore, it is important also to be able to predict the audio sound in the near field of a steerable PAL.

The challenge of calculating the audio sound in the near field of a PAL is to solve the nonlinear equation with a low computational load. The quasilinear solution of the Westervelt equation is usually used to obtain the audio sound.^{11,12} However, the expression is known to be very time-consuming to compute because it contains the numerical evaluation of five-fold integrals.¹² In 2021, Zhong *et al.* proposed a cylindrical expansion to obtain the audio sound generated by a steerable PAL based on the Westervelt equation, which simplifies the calculation into two-fold summations and integrals.⁷ Their results showed the expansion improved the agreement with the experimental results when

^{a)}Electronic mail: hszou@nju.edu.cn

compared to the convolution model. However, in this model one dimension of the PAL is assumed to be infinitely long, and this assumption is questionable at low audio frequencies because the size of a PAL is usually less than the audio wavelength, which might reduce prediction accuracy. Nevertheless, the spherical wave expansion (SWE) method is attractive because no additional approximations are required and this involves a relatively low computational expenditure.¹² In addition, the local effects determined by the ultrasonic Lagrangian density in the near field can also be correctly captured by the SWE, making it a useful tool to simulate both the near and far field of the audio sound.^{13,14} However, the limitations of the model mean it is valid only for a circular PAL with an axisymmetric velocity profile, which is not applicable for a steerable PAL as this has an asymmetric profile over the radiation surface.

The Gaussian beam expansion (GBE) may also be used to calculate the quasilinear solution of the Westervelt or Khokhlov-Zabolotskaya-Kuznetsov (KZK) equations.¹⁵ The mechanism is to approximate the velocity profile on the radiation surface by a set of Gaussian functions. The radiation from each Gaussian profile has a closed-form expression under the paraxial (Fresnel) approximation for both ultrasound and audio sound beams, so the calculation is simplified. However, it has been demonstrated that the GBE is inaccurate at low audio frequencies due to the paraxial approximation for audio sound.¹¹ Even at high audio frequencies, the paraxial approximation assumed for ultrasound results in significant inaccuracies when the sound beam is steered away from the radiator axis, because the main lobe of the ultrasonic beam lies away from the paraxial region. Moreover, since the Gaussian functions are not a complete set, the audio sound in the near field obtained using the GBE is inaccurate no matter how many Gaussian functions are used.¹⁶

An alternative approach should aim to replace a GBE with functions that form a complete set. One possible approach is to use Zernike circular polynomials as these are orthogonal and form a complete set over the interior of a unit circle.^{17,18} Therefore, any well-behaved function can be expanded as a series of functions of the set of Zernike polynomials. Accordingly, it is proposed here to compute the sound radiated by a steerable PAL using a Zernike profile, so that the sound field generated by a planar source with an arbitrary velocity profile can be obtained. Zernike polynomials have been extensively used in optics to approximate the aberration function.¹⁷ They have also been introduced in acoustics to solve various kinds of radiation problems, for example: radiation from circular sources,^{19–21} radiation from a spherical cap,²² radiation from a vibrating clamped circular plate,^{23,24} estimating the velocity profile of a loudspeaker,²⁵ and sound transmission through a circular aperture.²⁶ Contrary to the GBE, the radiation calculated using the Zernike polynomials is accurate for the entire frequency range in both the near and far fields. Therefore, in this article, Zernike polynomials, are used for the first time to calculate sound radiation from a steerable radiator.

In this paper, the steerable profile on the radiation surface of a circular steerable PAL is expanded as a set of Zernike circular polynomials. The closed-form expressions of the expansion coefficients are developed and presented. An extension of the SWE is developed to efficiently calculate the quasilinear solution of the audio sound generated by a PAL using a Zernike profile. The proposed expansion is further extended to accommodate local effects by using an algebraic correction to Westervelt equation.²⁷ The transition distance that describes if the local effects are significant for a steerable PAL is also investigated. Numerical results with a steerable PAL generating single and dual beams are then presented and discussed.

II. QUASILINEAR SOLUTION

A. Physical model

As shown in Fig. 1, a circular steerable PAL is investigated in this paper. The radius of the PAL is denoted by a . A Cartesian coordinate system (x, y, z) is established with its origin, O , at the center of the PAL, with the positive z axis pointing along the radiator axis. The spherical coordinate system (r, θ, φ) is established with respect to the Cartesian coordinates for further calculations, where r , θ , and φ are the radial distance, zenith angle, and azimuth angle, respectively.

When the ultrasound at the frequencies of f_1 and f_2 ($f_1 > f_2$) is radiated by the PAL, the audio sound with the frequency of $f_a = f_1 - f_2$ is demodulated due to the second-order nonlinearity caused by air. The excitation velocity profile on the transducer surface is assumed to be asymmetric as

$$u(r_s, \varphi_s, t) = u_1(r_s, \varphi_s)e^{-i\omega_1 t} + u_2(r_s, \varphi_s)e^{-i\omega_2 t}, \quad 0 \leq r_s \leq a, \quad (1)$$

where i is the imaginary unit, r_s and φ_s are the radial and azimuthal coordinates of a source point $\mathbf{r}_s = (x_s, y_s, 0)$ on the radiation surface, the corresponding zenithal coordinate $\theta_s = \pi/2$, the angular frequency $\omega_i = 2\pi f_i$, t is the time, $u_i(r_s, \varphi_s)$ is the excitation velocity profile at f_i . Here and in the sequel, the subscript $i = 1, 2$ denotes the ultrasound index.

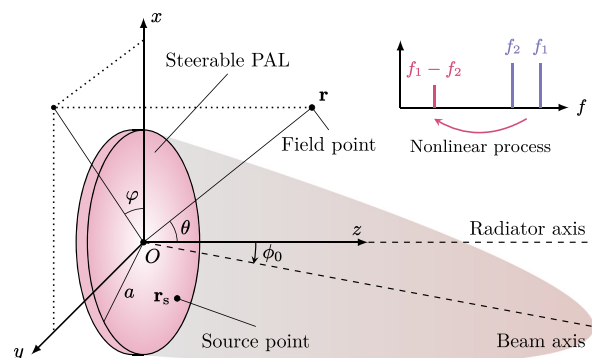


FIG. 1. (Color online) Sketch of a circular steerable PAL.

In this paper, the steerable PAL is realized by applying a continuous profile for the ultrasound, i.e.,⁷

$$u_i(r, \varphi) = u_0 \exp[i \operatorname{Re}(k_i) r \cos \varphi \sin \phi_0], \quad 0 \leq r \leq a, \quad (2)$$

where u_0 is a real constant, $\operatorname{Re}(\cdot)$ denotes the real part of the argument, the complex wavenumber $k_i = \omega_i/c_0 + i\alpha_i$, c_0 is the sound speed, α_i is the sound attenuation coefficient at f_i , and the steering angle $-\pi/2 \leq \phi_0 \leq \pi/2$. The geometric illustration of the steering angle can be seen in Fig. 1. When $\phi_0 = 0$, it indicates that the steerable PAL becomes a conventional PAL so that the beam direction is perpendicular to the radiation surface. When $\phi_0 > 0$, it indicates the beam is steered to the positive side of the x axis; and negative side of the x axis for $\phi_0 < 0$.

In some cases, it is required to steer multiple beams into multiple directions.^{5,28} This can be realized by applying the profile as

$$u_i(r, \varphi) = \sum_{j=1}^J u_0 \exp[i \operatorname{Re}(k_i) r \cos \varphi \sin \phi_j], \quad 0 \leq r \leq a, \quad (3)$$

where J is the total number of steered beams, and ϕ_j denotes the j -th steering angle.

The challenge of modelling a steerable PAL is to obtain accurate numerical results with a low computational load. Existing methods based on the Westervelt and KZK equations usually adopt a paraxial assumption,¹¹ indicating that only the ultrasound near the radiator axis is correctly captured for calculating the audio sound. When the audio beam is steered at an angle, the ultrasonic beam is outside of the paraxial region leading to a significant reduction in prediction accuracy for the audio sound. In the following text, the quasilinear solutions of the Westervelt equation with and without local effects are presented and the SWE will be developed without additional approximations by using Zernike polynomials.

B. Quasilinear solution without local effects

When local effects are neglected, the radiation of sound from a PAL is governed by the Westervelt equation^{29,30}

$$\nabla^2 p - \frac{1}{c_0^2} \frac{\partial^2 p}{\partial t^2} = -\frac{\delta}{c_0^2} \nabla^2 \frac{\partial p}{\partial t} - \frac{\beta}{\rho_0 c_0^4} \frac{\partial^2 p^2}{\partial t^2}, \quad (4)$$

where p is the sound pressure, δ is the sound diffusivity parameter related to the sound attenuation coefficient, $\beta = 1.2$ is the nonlinearity coefficient in air, and ρ_0 is the air density.

By using the quasilinear approximation and the successive method, the nonlinear Westervelt equation is decomposed into two coupled linear wave equations taking the form of¹³

$$\begin{cases} (\nabla^2 + k_i^2) p_i(\mathbf{r}) = 0 \\ (\nabla^2 + k_a^2) p_a(\mathbf{r}) = q(\mathbf{r}), \end{cases} \quad (5)$$

where $p_i(\mathbf{r})$ is the ultrasound pressure at the frequency of f_i , the wavenumber for audio sound $k_a = \omega_a/c_0 + i\alpha_a$, $\omega_a = 2\pi f_a$, α_a is the sound absorption coefficient at f_a , $p_a(\mathbf{r})$ is the audio sound pressure, and $q(\mathbf{r})$ is the source density proportional to the product of ultrasound pressure expressed as¹³

$$q(\mathbf{r}) = \frac{\beta \omega_a}{i \rho_0^2 c_0^4} p_1(\mathbf{r}) p_2^*(\mathbf{r}). \quad (6)$$

In Eq. (6), the asterisk denotes the complex conjugate. The ultrasound pressure can be modelled as the radiation from a baffled circular source using the Rayleigh integral so that¹²

$$p_i(\mathbf{r}) = -2i \rho_0 c_0 k_i \int_0^{2\pi} \int_0^a u_i(r_s, \varphi_s) g(\mathbf{r}, \mathbf{r}_s, k_i) r_s dr_s d\varphi_s, \quad (7)$$

where $g(\mathbf{r}, \mathbf{r}_s, k_i)$ is the free field Green's function between the field point \mathbf{r} and the source point \mathbf{r}_s at a wavenumber of k_i , which is expressed as

$$g(\mathbf{r}, \mathbf{r}_s, k_i) = \frac{\exp(ik_i |\mathbf{r} - \mathbf{r}_s|)}{4\pi |\mathbf{r} - \mathbf{r}_s|}. \quad (8)$$

The audio sound can be seen as the radiation from an infinitely large volume source with a source density given by Eq. (6). Therefore, the audio sound pressure based on the Westervelt equation is obtained as¹²

$$p_a(\mathbf{r}) = -i \rho_0 c_0 k_a \iiint_V q(\mathbf{r}_v) g(\mathbf{r}, \mathbf{r}_v, k_a) d^3 \mathbf{r}_v, \quad (9)$$

where V represents the full space to be integrated.

C. Quasilinear solution with local effects

The Westervelt equation given by Eq. (4) is only accurate in the Westervelt far field, as demonstrated by Zhong *et al.*¹³ To obtain an accurate prediction of audio sound in the near field, the so-called “local effects” must be considered, which are determined by the Lagrangian density of ultrasound.^{13,29,30} Existing methods usually adopt the second-order nonlinear wave equation or the Kuznetsov equation to include the local effects.^{13,29,31} Recently, an algebraic correction to the quasilinear solution of the Westervelt equation was proposed to correct the local effects.²⁷ This correction is more computationally efficient, so it is used here and reads

$$\begin{aligned} \tilde{p}_a(\mathbf{r}) = & p_a(\mathbf{r}) - \left[\frac{\rho_0}{2} \mathbf{v}_1(\mathbf{r}) \cdot \mathbf{v}_2^*(\mathbf{r}) - \left(\frac{\omega_1}{\omega_2} + \frac{\omega_2}{\omega_1} - 1 \right) \right. \\ & \left. \times \frac{p_1(\mathbf{r}) p_2^*(\mathbf{r})}{2 \rho_0 c_0^2} \right], \end{aligned} \quad (10)$$

where $\mathbf{v}_i(\mathbf{r})$ is the particle velocity of ultrasound at the frequency of f_i . It can be obtained by using the linear relation to the ultrasound pressure as

$$\mathbf{v}_i(\mathbf{r}) = \frac{\nabla p_i(\mathbf{r})}{i\rho_0\omega_i}. \quad (11)$$

It is well known that the Westervelt equation cannot capture the complex interactions of ultrasound resulting in the local effects in the near field and the prediction accuracy is therefore deteriorated.^{13,29} It is then necessary to find the transition distance determining whether the local effects are significant or not. An estimation of the transition distance was given by Eq. (35) in Ref. 13, and for a conventional PAL this yields

$$r_0 = \frac{a^2}{\lambda_u} - \frac{\lambda_u}{4}, \quad (12)$$

where λ_u is the ultrasonic wavelength at the center frequency $f_u = (f_1 + f_2)/2$. It is noted that in most cases $\lambda_u/4$ is much less than a^2/λ_u , so a^2/λ_u is sufficiently accurate to indicate the transition distance. Beyond the transition distance, the quasilinear solution of the Westervelt equation given by Eq. (7) can then be used for prediction without large errors. However, in the near field before the transition distance this should be corrected using Eq. (10), which requires larger computational load. This is examined in this paper to verify whether it is still valid for a steerable PAL.

III. SPHERICAL WAVE EXPANSION USING ZERNIKE POLYNOMIALS

In this section, the Zernike expansion of the steerable profile for ultrasound is derived first in Sec. III A. Then the SWE of both the ultrasound pressure and particle velocity with a Zernike profile is derived in Sec. III B. The SWE for calculating the audio sound with and without local effects is derived and presented in Sec. III C. Finally, the special case when the steerable PAL becomes a conventional PAL is presented in Sec. III D to show the proposed method is an extension of the SWE proposed in Refs. 12 and 13.

A. Zernike expansion of the steerable profile

The steerable profile given by Eq. (2) can be decomposed into summation of Zernike circular polynomials as¹⁸

$$u_i(r, \varphi) = \sum_{n_i=0}^{\infty} \sum_{m_i=-n_i}^{n_i} M_{n_i}^{m_i} R_{n_i}^{m_i}(r/a) e^{im_i\varphi}, \quad (13)$$

where the prime over the summation sign indicates that the summation is performed for terms only when $n_i - m_i$ is even, $R_{n_i}^{m_i}(r/a)$ is the radial polynomial of degree n_i and azimuthal order m_i defined as, see Eq. (2.3) in Ref. 32,

$$R_{n_i}^{m_i}(\sigma) = \sum_{l=0}^{(n_i-|m_i|)/2} \frac{(-1)^l (n_i - l)!}{l! \left(\frac{n_i + |m_i|}{2} - l\right)! \left(\frac{n_i - |m_i|}{2} - l\right)!} \sigma^{n_i-2l}, \quad (14)$$

where $\sigma = r/a$ ranges from 0 to 1, “!” denotes the factorial, and $M_{n_i}^{m_i}$ are the coefficients (also known as Zernike moments), see Eq. (8) in Ref. 18,

$$M_{n_i}^{m_i} = \frac{n_i + 1}{\pi} \int_0^1 \int_0^{2\pi} u_i(a\sigma, \varphi) R_{n_i}^{m_i}(\sigma) e^{-im_i\varphi} \sigma d\sigma d\varphi. \quad (15)$$

According to the integral representation of Bessel functions, given by Eq. (9.1.21) in Ref. 33, we obtain

$$\frac{1}{2\pi} \int_0^{2\pi} \exp\{i[\text{Re}(k_i)a\sigma \cos \varphi \sin \phi_0 - m_i\varphi]\} d\varphi = i^{m_i} J_{m_i}(\text{Re}(k_i)a\sigma \sin \phi_0), \quad (16)$$

where $J_m(\cdot)$ is the Bessel function of order m . The substitution of Eqs. (2) and (16) into Eq. (15) yields

$$M_{n_i}^{m_i} = 2(n_i + 1) i^{m_i} u_0 \int_0^1 R_{n_i}^{m_i}(\sigma) J_{m_i}(\text{Re}(k_i)a\sigma \sin \phi_0) \sigma d\sigma. \quad (17)$$

By using the integral relation given by Eq. (9) in Sec. 9.2 of Ref. 17,

$$\int_0^1 R_{n_i}^{m_i}(\sigma) J_{m_i}(ka\sigma \sin \phi_0) \sigma d\sigma = i^{n_i-m_i} \frac{J_{n_i+1}(\text{Re}(k_i)a \sin \phi_0)}{\text{Re}(k_i)a \sin \phi_0}, \quad (18)$$

Eq. (17) then reduces to the closed-form expression

$$M_{n_i} = 2(n_i + 1) i^{n_i} u_0 \frac{J_{n_i+1}(\text{Re}(k_i)a \sin \phi_0)}{\text{Re}(k_i)a \sin \phi_0}. \quad (19)$$

Note that Eq. (19) is independent of m_i , so the notation $M_{n_i}^{m_i}$ may be simplified to M_{n_i} . By substituting Zernike moments given by Eq. (19) into the Zernike expansion given by Eq. (13), the velocity profile can then be obtained, which is identical to Eq. (2).

B. Ultrasound

By using the Zernike expansion for the velocity profile given by Eq. (13), the ultrasound is the superposition of the radiation from each Zernike mode, so that

$$p_i(\mathbf{r}) = \sum_{n_i=0}^{\infty} \sum_{m_i=-n_i}^{n_i} M_{n_i} p_{n_i}^{m_i}(\mathbf{r}), \quad (20)$$

where $p_{n_i}^{m_i}(\mathbf{r})$ is the sound pressure radiated by the source with a Zernike profile $R_{n_i}^{m_i}(r/a) e^{im_i\varphi}$. To solve for $p_{n_i}^{m_i}(\mathbf{r})$, the Green's function given by Eq. (8) is expressed in spherical coordinates as [see Eqs. (2.49) and (2.50) in Ref. 34]

$$g(\mathbf{r}, \mathbf{r}_s, k_i) = ik_i \sum_{\ell_i=0}^{\infty} j_{\ell_i}(k_i r_{s,<}) h_{\ell_i}(k_i r_{s,>}) \sum_{m=-\ell_i}^{\ell_i} Y_{\ell_i}^m(\theta, \varphi) Y_{\ell_i}^m(\theta_s, -\varphi_s), \quad (21)$$

where the symmetric relation $[Y_{\ell_i}^m(\theta_s, \varphi_s)]^* = Y_{\ell_i}^m(\theta_s, -\varphi_s)$ has been used for further calculation, $j_{\ell_i}(\cdot)$ and $h_{\ell_i}(\cdot)$ are the spherical Bessel and Hankel functions of order ℓ_i , respectively, $Y_{\ell_i}^m(\theta, \varphi)$ is the spherical harmonic, $r_{s,<} = \min(r, r_s)$, $r_{s,>} = \max(r, r_s)$, and it is noted that $\theta_s = \pi/2$. By substituting Eq. (21) into the Rayleigh integral given by Eq. (7), the ultrasound pressure generated by a circular source with the Zernike profile of mode (n_i, m_i) is obtained as

$$p_{n_i}^{m_i}(\mathbf{r}) = 2p_0 \sum_{\ell_i=0}^{\infty} \left[\int_0^a R_{n_i}^{m_i}(r_s/a) j_{\ell_i}(k_i r_{s,<}) h_{\ell_i}(k_i r_{s,>}) k_i^2 r_s dr_s \right] \sum_{m=-\ell_i}^{\ell_i} Y_{\ell_i}^m(\theta, \varphi) \int_0^{2\pi} Y_{\ell_i}^m(\pi/2, -\varphi_s) e^{im_i \varphi_s} d\varphi_s, \quad (22)$$

where $\theta_s = \pi/2$ has been used and $p_0 = \rho_0 c_0 u_0$. By using the integral

$$\int_0^{2\pi} Y_{\ell_i}^m(\pi/2, -\varphi_s) e^{im_i \varphi_s} d\varphi_s = 2\pi Y_{\ell_i}^{m_i}(\pi/2, 0) \delta_{m,m_i}, \quad (23)$$

where δ_{m,m_i} is the Kronecker delta function, Eq. (22) reduces to

$$p_{n_i}^{m_i}(\mathbf{r}) = 4\pi p_0 \sum_{\ell_i=0}^{\infty} \left[\int_0^a R_{n_i}^{m_i}(r_s/a) j_{\ell_i}(k_i r_{s,<}) h_{\ell_i}(k_i r_{s,>}) k_i^2 r_s dr_s \right] Y_{\ell_i+|m_i|}^{m_i}(\theta, \varphi) Y_{\ell_i+|m_i|}^{m_i}(\pi/2, 0), \quad (24)$$

where $\ell_i + |m_i|$ has been used to replace the original index ℓ_i . According to Eq. (11) in Ref. 12, $Y_{\ell_i+|m_i|}^{m_i}(\pi/2, 0)$ is non-zero only when ℓ_i is even. By substituting the original ℓ_i with $2\ell_i$ to eliminate the odd terms, Eq. (24) can be written as

$$p_{n_i}^{m_i}(\mathbf{r}) = 4\pi p_0 \sum_{\ell_i=0}^{\infty} \mathcal{R}_{2\ell_i+|m_i|}^{n_i, m_i}(r) Y_{2\ell_i+|m_i|}^{m_i}(\theta, \varphi) Y_{2\ell_i+|m_i|}^{m_i}(\pi/2, 0), \quad (25)$$

where the radial component for ultrasound is

$$\mathcal{R}_{2\ell_i+|m_i|}^{n_i, m_i}(r) = \int_0^a R_{n_i}^{m_i}(r_s/a) j_{2\ell_i+|m_i|}(k_i r_{s,<}) h_{2\ell_i+|m_i|}(k_i r_{s,>}) k_i^2 r_s dr_s. \quad (26)$$

The ultrasonic particle velocity is required in Eq. (10). By substituting Eq. (25) into Eq. (11), the velocity components in spherical coordinates can be obtained, which yields

$$\begin{cases} v_{r,n_i}^{m_i}(\mathbf{r}) = \frac{1}{i\rho_0 c_0 k_i} \frac{\partial p_{n_i}^{m_i}(\mathbf{r})}{\partial r} = -4\pi i u_0 \sum_{\ell_i=0}^{\infty} \frac{\mathcal{R}_{2\ell_i+|m_i|}^{n_i, m_i}(r)}{d(k_i r)} Y_{2\ell_i+|m_i|}^{m_i}(\theta, \varphi) Y_{2\ell_i+|m_i|}^{m_i}(\pi/2, 0), \\ v_{\theta,n_i}^{m_i}(\mathbf{r}) = \frac{1}{i\rho_0 c_0 k_i r} \frac{\partial p_{n_i}^{m_i}(\mathbf{r})}{\partial \theta} = -4\pi i u_0 \sum_{\ell_i=0}^{\infty} \frac{\mathcal{R}_{2\ell_i+|m_i|}^{n_i, m_i}(r)}{k_i r} \frac{\partial Y_{2\ell_i+|m_i|}^{m_i}(\theta, \varphi)}{\partial \theta} Y_{2\ell_i+|m_i|}^{m_i}(\pi/2, 0), \\ v_{\varphi,n_i}^{m_i}(\mathbf{r}) = \frac{1}{i\rho_0 c_0 k_i r \sin \theta} \frac{\partial p_{n_i}^{m_i}(\mathbf{r})}{\partial \varphi} = -4\pi i u_0 \sum_{\ell_i=0}^{\infty} \frac{\mathcal{R}_{2\ell_i+|m_i|}^{n_i, m_i}(r)}{k_i r \sin \theta} \frac{\partial Y_{2\ell_i+|m_i|}^{m_i}(\theta, \varphi)}{\partial \varphi} Y_{2\ell_i+|m_i|}^{m_i}(\pi/2, 0), \end{cases} \quad (27)$$

where the derivative of the spherical harmonic with respect to the zenithal angle can be obtained by using the properties of the associated Legendre functions³⁵

$$\frac{\partial Y_{\nu}^{\mu}(\theta, \varphi)}{\partial \theta} = \mu \cot \theta Y_{\nu}^{\mu}(\theta, \varphi) + \sqrt{(\nu - \mu)(\nu + \mu + 1)} Y_{\nu}^{\mu+1}(\theta, \varphi) e^{-i\varphi}. \quad (28)$$

C. Audio sound

The source density contributed by the ultrasound with the Zernike profile of mode (n_i, m_i) at f_i is obtained by substituting Eq. (25) into Eq. (6) as

$$\begin{aligned} q_{\mathbf{n}}^{\mathbf{m}}(\mathbf{r}_{\mathbf{v}}) &= \frac{16\pi^2 \beta \omega_a p_0^2}{i\rho_0^2 c_0^4} \sum_{\ell_1, \ell_2=0}^{\infty} Y_{2\ell_1+|m_1|}^{m_1}(\pi/2, 0) Y_{2\ell_2+|m_2|}^{m_2}(\pi/2, 0) \\ &\quad \times \mathcal{R}_{2\ell_1+|m_1|}^{n_1, m_1}(r_{\mathbf{v}}) \left[\mathcal{R}_{2\ell_2+|m_2|}^{n_2, m_2}(r_{\mathbf{v}}) \right]^* Y_{2\ell_1+|m_1|}^{m_1}(\theta_{\mathbf{v}}, \varphi_{\mathbf{v}}) \left[Y_{2\ell_2+|m_2|}^{m_2}(\theta_{\mathbf{v}}, \varphi_{\mathbf{v}}) \right]^*, \end{aligned} \quad (29)$$

where the index sets $\mathbf{n} = (n_1, n_2)$ and $\mathbf{m} = (m_1, m_2)$ are used for simplicity. The substitution of Eqs. (21) and (29) into Eq. (9) yields the audio sound pressure of the mode (\mathbf{n}, \mathbf{m}) as

$$p_{\mathbf{n}}^{\mathbf{m}}(\mathbf{r}) = \frac{16\pi^2 \beta p_0^2}{i\rho_0 c_0^2} \sum_{\ell_1, \ell_2=0}^{\infty} Y_{2\ell_1+|m_1|}^{m_1}(\pi/2, 0) Y_{2\ell_2+|m_2|}^{m_2}(\pi/2, 0) \sum_{\ell_3=0}^{\infty} \sum_{m_3=-\ell_3}^{\ell_3} Y_{\ell_3}^{m_3}(\theta, \varphi) \\ \times \int_0^{\infty} j_{\ell_3}(k_a r_{v,<}) h_{\ell_3}(k_a r_{v,>}) \mathcal{R}_{2\ell_1+|m_1|}^{n_1, m_1}(r_v) [\mathcal{R}_{2\ell_2+|m_2|}^{n_2, m_2}(r_v)]^* k_a^3 r_v^2 dr_v \\ \times \int_0^{2\pi} \int_0^{\pi} Y_{2\ell_1+|m_1|}^{m_1}(\theta_v, \varphi_v) Y_{2\ell_2+|m_2|}^{m_2}(\theta_v, -\varphi_v) Y_{\ell_3}^{m_3}(\theta_v, -\varphi_v) \sin \theta_v d\theta_v d\varphi_v, \quad (30)$$

$r_{v,<} = \min(r, r_v)$, and $r_{v,>} = \max(r, r_v)$. According to the integration of triple spherical harmonics, which has been studied extensively in the quantum mechanics, see Eq. (B.2) in Ref. 36,

$$\int_0^{2\pi} \int_0^{\pi} Y_{2\ell_1+|m_1|}^{m_1}(\theta_v, \varphi_v) Y_{2\ell_2+|m_2|}^{m_2}(\theta_v, -\varphi_v) Y_{\ell_3}^{m_3}(\theta_v, -\varphi_v) \sin \theta_v d\theta_v d\varphi_v \\ = (-1)^{m_1} \sqrt{\frac{(4\ell_1+2|m_1|+1)(4\ell_2+2|m_2|+1)(2\ell_3+1)}{4\pi}} \\ \times \begin{pmatrix} 2\ell_1+|m_1| & 2\ell_2+|m_2| & \ell_3 \\ 0 & 0 & 0 \end{pmatrix} \begin{pmatrix} 2\ell_1+|m_1| & 2\ell_2+|m_2| & \ell_3 \\ m_1 & -m_2 & -m_3 \end{pmatrix} \delta_{m_3, m_1-m_2}, \quad (31)$$

where the relation $Y_{\nu}^{\mu}(\theta_v, -\varphi_v) = (-1)^{\mu} Y_{\nu}^{-\mu}(\theta_v, \varphi_v)$ has been used, and $\begin{pmatrix} j_1 & j_2 & j_3 \\ \mu_1 & \mu_2 & \mu_3 \end{pmatrix}$ is the Wigner $3j$ symbol.¹³ It is known that the Wigner $3j$ symbol vanishes unless $\mu_1 + \mu_2 + \mu_3 = 0$, which is consistent with the Kronecker delta function δ_{m_3, m_1-m_2} due to the orthogonality of $\{e^{im\varphi_v}\}$. The Wigner $3j$ symbol also vanishes unless the triangle inequality holds, i.e., $|j_1 - j_2| \leq j_3 \leq j_1 + j_2$. The substitution of Eq. (31) into Eq. (30) yields

$$p_{\mathbf{n}}^{\mathbf{m}}(\mathbf{r}) = \frac{16\pi^2 \beta p_0^2}{i\rho_0 c_0^2} \sum_{\ell=0}^{\infty} Y_{2\ell_1+|m_1|}^{m_1}(\pi/2, 0) Y_{2\ell_2+|m_2|}^{m_2}(\pi/2, 0) Y_{\ell_3+|m_-|}^{m_-}(\theta, \varphi) \\ \times \int_0^{\infty} j_{\ell_3+|m_-|}(k_a r_{v,<}) h_{\ell_3+|m_-|}(k_a r_{v,>}) \mathcal{R}_{2\ell_1+|m_1|}^{n_1, m_1}(r_v) [\mathcal{R}_{2\ell_2+|m_2|}^{n_2, m_2}(r_v)]^* k_a^3 r_v^2 dr_v \\ \times (-1)^{m_1} \sqrt{\frac{(4\ell_1+2|m_1|+1)(4\ell_2+2|m_2|+1)(2\ell_3+2|m_-|+1)}{4\pi}} \\ \times \begin{pmatrix} 2\ell_1+|m_1| & 2\ell_2+|m_2| & \ell_3+|m_-| \\ 0 & 0 & 0 \end{pmatrix} \begin{pmatrix} 2\ell_1+|m_1| & 2\ell_2+|m_2| & \ell_3+|m_-| \\ m_1 & -m_2 & -m_- \end{pmatrix}, \quad (32)$$

where $m_- = m_1 - m_2$, $\ell_3 + |m_-|$ has been used to replace the original index ℓ_3 , and ℓ stands for the index set of (ℓ_1, ℓ_2, ℓ_3) for simplicity.

When $\mu_1 = \mu_2 = \mu_3 = 0$, the Wigner $3j$ symbol vanishes unless $j_1 + j_2 + j_3$ is even as shown in Eq. (20) of Ref. 12. Therefore, only the terms in Eq. (32) when ℓ_3 is even are retained. By substituting the original ℓ_3 with $2\ell_3$ to eliminate the odd terms, Eq. (32) can be written as

$$p_{\mathbf{n}}^{\mathbf{m}}(\mathbf{r}) = \frac{16\pi^2 \beta p_0^2}{i\rho_0 c_0^2} \sum_{\ell=0}^{\infty} A_{\ell}^{\mathbf{m}} \chi_{\ell}^{\mathbf{n}, \mathbf{m}}(r) Y_{2\ell_3+|m_-|}^{m_-}(\theta, \varphi), \quad (33)$$

where the radial component for audio sound is defined as

$$\chi_{\ell}^{\mathbf{n}, \mathbf{m}}(r) = \int_0^{\infty} j_{2\ell_3+|m_-|}(k_a r_{v,<}) h_{2\ell_3+|m_-|}(k_a r_{v,>}) \mathcal{R}_{2\ell_1+|m_1|}^{n_1, m_1}(r_v) [\mathcal{R}_{2\ell_2+|m_2|}^{n_2, m_2}(r_v)]^* k_a^3 r_v^2 dr_v \quad (34)$$

and the coefficient is

$$A_{\ell}^{\mathbf{m}} = (-1)^{m_1} Y_{2\ell_1+|m_1|}^{m_1}(\pi/2, 0) Y_{2\ell_2+|m_2|}^{m_2}(\pi/2, 0) \times \sqrt{\frac{(4\ell_1+2|m_1|+1)(4\ell_2+2|m_2|+1)(4\ell_3+2|m_-|+1)}{4\pi}} \\ \times \begin{pmatrix} 2\ell_1+|m_1| & 2\ell_2+|m_2| & 2\ell_3+|m_-| \\ 0 & 0 & 0 \end{pmatrix} \begin{pmatrix} 2\ell_1+|m_1| & 2\ell_2+|m_2| & 2\ell_3+|m_-| \\ m_1 & -m_2 & -m_- \end{pmatrix}. \quad (35)$$

Equation (33) is the main result of this paper, which is a computationally efficient expression similar to those proposed using an SWE in Refs. 12 and 13. The radial component given by Eq. (34) can be efficiently computed using the complex continuation method introduced in Ref. 12. The Wigner 3j symbol required in Eq. (35) can be calculated using Eq. (20) in Ref. 12 and the Racah formula, see Eq. (C.21) in Ref. 37. After calculating Eq. (33) using Eqs. (34) and (35), the audio sound pressure can then be obtained as

$$p(\mathbf{r}) = \sum_{n=0}^{\infty} \sum_{m=-n}^n M_{n_1} M_{n_2}^* p_n^m(\mathbf{r}). \quad (36)$$

In the numerical computations, it is noted that the audio sound pressure generated by a PAL with Zernike profiles at different modes, $p_n^m(\mathbf{r})$, can be calculated first and saved as a table. Then the total audio sound pressure at different steering angles can be obtained by using this table and Zernike moments M_{n_i} obtained by Eq. (19).

D. Degenerated case: A piston source

When the steering angle is zero, the steerable PAL becomes a conventional PAL radiated by a piston source. By setting $\phi_0 = 0$ in Eq. (2), the velocity profile reduces to

$$u_i(r, \varphi) = u_0, \quad r \leq a. \quad (37)$$

From Eq. (19), it can be found Zernike moments M_{n_i} are non-zero only when $n_i = 0$ and $M_0 = 1$, indicating that the ultrasound pressure reduces to

$$p_i(\mathbf{r}) = M_0 p_0^0(\mathbf{r}) = p_0^0(\mathbf{r}), \quad (38)$$

where the ultrasound at mode (0, 0) is obtained by Eq. (25) as

$$p_0^0(\mathbf{r}) = 4\pi p_0 \sum_{\ell_i=0}^{\infty} \mathcal{R}_{2\ell_i}^{0,0}(r) Y_{2\ell_i}^0(\theta, \varphi) Y_{2\ell_i}^0(\pi/2, 0). \quad (39)$$

The radial component for ultrasound is simplified from Eq. (26) as

$$\mathcal{R}_{2\ell_i}^{0,0}(r) = \int_0^a j_{2\ell_i}(k_i r_{s,<}) h_{2\ell_i}(k_i r_{s,>}) k_i^2 r_s dr_s, \quad (40)$$

where the special value $R_0^0(\sigma) = 1$ has been used. It can be seen that Eq. (40) is the same as Eq. (14) in Ref. 12. By expanding the spherical harmonics into Legendre functions, it can be shown Eq. (39) is also identical to Eq. (12) in Ref. 12.

According to Eq. (36), the audio sound is contributed only from the ultrasound of mode (0, 0). By using Eq. (33), the audio sound pressure is obtained as

$$p(\mathbf{r}) = p_{0,0}^0(\mathbf{r}) = \frac{16\pi^2 \beta p_0^2}{i \rho_0 c_0^2} \sum_{\ell=0}^{\infty} A_{0,0,0}^{0,0} \chi_{0,0,0}^{0,0,0}(r) Y_{2\ell}^0(\theta, \varphi). \quad (41)$$

According to Eq. (34), the radial component for audio sound is

$$\chi_{0,0,0}^{0,0,0}(r) = \int_0^{\infty} j_{2\ell_3}(k_a r_{v,<}) h_{2\ell_3}(k_a r_{v,>}) \times \mathcal{R}_{2\ell_1}^{0,0}(r_v) [\mathcal{R}_{2\ell_2}^{0,0}(r_v)]^* k_a^3 r_v^2 dr_v, \quad (42)$$

which is the same as Eq. (22) in Ref. 12. The coefficient can be obtained by Eq. (35) as

$$A_{0,0,0}^{0,0} = Y_{2\ell_1}^0(\pi/2, 0) Y_{2\ell_2}^0(\pi/2, 0) \times \sqrt{\frac{(4\ell_1+1)(4\ell_2+1)(4\ell_3+1)}{4\pi}} \times \begin{pmatrix} 2\ell_1 & 2\ell_2 & 2\ell_3 \\ 0 & 0 & 0 \end{pmatrix}^2. \quad (43)$$

By expanding the spherical harmonics into Legendre functions, Eq. (41) is identical to Eq. (21) in Ref. 12 after the substitution of Eq. (43). The SWE presented in Ref. 12 is applicable only for a circular PAL with a uniform profile, which corresponds to Zernike mode (0,0) for the generalized model developed in this work. This means that the Zernike mode (0,0) predictions exactly match those presented in Ref. 12 for a circular PAL with a uniform profile. In other words, the proposed SWE is an extension of the SWE in Ref. 12.

IV. NUMERICAL RESULTS

Numerical simulations are conducted in MATLAB R2022a (MathWorks, Natick, MA). The center frequency of the ultrasound is set as $f_u = 40$ kHz. The sound attenuation coefficient, α_u , at 40 kHz is approximately 0.15 Np/m calculated according to ISO 9613-1 with a relative humidity of 70% and temperature of 20 °C. The radius of the PAL is set as $a = 0.04$ m. The transition distance from the near field to the Westervelt far field for the audio sound is 0.19 m calculated by Eq. (12). The Rayleigh distance is 0.59 m. The vibration velocity profile constant u_0 is set as 0.3 m/s for all cases. The reference pressure for the sound pressure level (SPL) is 20 μ Pa. The sound field on the xOz plane ($y = 0$) is presented for all following figures. The accuracy of the Zernike expansion of the steerable profile is examined in

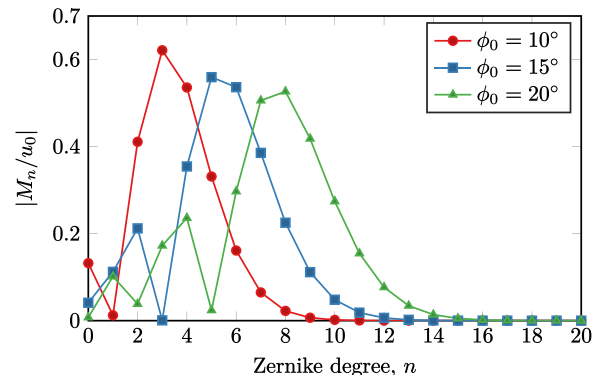


FIG. 2. (Color online) The magnitude of Zernike moments of different degrees n and steering angles ϕ_0 at the frequency of 40 kHz.

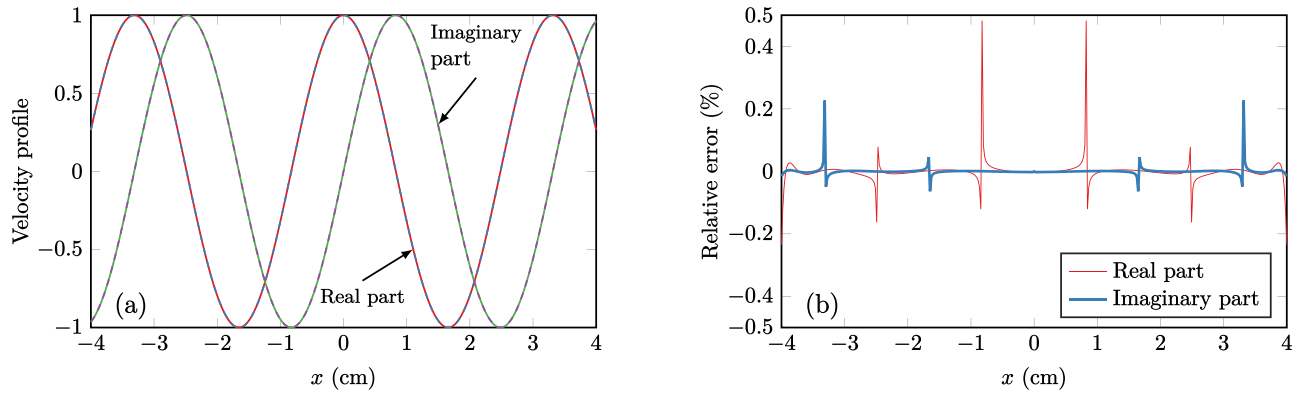


FIG. 3. (Color online) Comparison of the steerable profile at $y=0$ and the approximation using leading 15 terms of Zernike circular polynomials, where the ultrasound at 40 kHz is steered at the angle of $\phi_0 = 15^\circ$. The results are normalized to u_0 . (a) The velocity profile: solid line, the exact result obtained using Eq. (2); dashed line, the approximation result obtained using Eq. (13). (b) The relative error of the approximation.

Sec. IV A. The steerable ultrasound field is presented and analyzed in Sec. IV B. The steerable PAL generating single and dual beams is given in Secs. IV C and IV D, respectively.

A. Zernike expansion of the steerable profile

Figure 2 represents the magnitude of Zernike moments given by Eq. (19) of different degree n and the steering angle at the frequency of 40 kHz. It is seen that the magnitude has a peak, then decreases as the degree increases, and finally converges to zero. When the steering angle is 10° , 15° , and 20° , the magnitude is found to be less than 0.01 when the degree is larger than 8, 11, and 14, respectively. It shows the steerable profile can be approximated by the superposition of the profiles with several leading terms of Zernike polynomials.

Figure 3 gives an example of approximating the steerable profile at $y=0$ using 15 terms of Zernike circular polynomials when the ultrasound at 40 kHz is steered at the angle of $\phi_0 = 15^\circ$. The exact result is directly obtained using the closed-form expression given by Eq. (2) and presented for comparison. It is observed in Fig. 3(a) that an approximation of the velocity profile obtained using Eq. (13) agrees well with the exact result. Figure 3(b) presents the relative percentage error defined as $(\tilde{u} - u)/u \times 100\%$, where u and \tilde{u} are the real or imaginary parts of the exact result and the approximation of the velocity profile, respectively. The relative error is seen to be less than 0.5% in this case, so that the steerable profile is well approximated by the Zernike polynomials.

B. Steerable ultrasound field

To examine the accuracy of the ultrasound field when the steerable profile is approximated by the Zernike polynomials, the ultrasound pressure at several typical points is presented in Fig. 4 as a function of the Zernike degree n . It can be found the SPL at all points converges as the degree increases. The numerical results show that the error is less than 0.1 dB when the degree is more than 10. Contrary to

the paraxial approximation assumed in the GBE,¹¹ it is noted that the ultrasound field calculated by the SWE using Zernike polynomials converges towards the exact solution of the Rayleigh integral given by Eq. (7). In the following text, the truncation terms of the Zernike polynomials are set to 15 to ensure an accurate prediction of the ultrasound field.

Figure 5 shows the ultrasound field at 40 kHz steered at the angle of 15° . For comparison, the ultrasound field steered at the angle of 0° , i.e., without the beam steering, is also presented. Figure 6 presents the radial SPL along the beam direction and the angular SPL at a radial distance of 1 m for these two cases. It is noted that the azimuthal angle φ can be either 0° or 180° in the plane xOz , so the angular PAL as a function of $\theta \cos \varphi$ is presented in Fig. 6(b). When the ultrasonic beam is not steered, i.e., $\phi_0 = 0^\circ$, the energy is focused in the radiator direction. When the ultrasonic beam is steered at the angle of 15° , it is clear that the main lobe lies in the beam direction. It is noted in Fig. 6(a) that the SPL difference of these two cases is negligible when the radial distance is larger than the location of the last minimal SPL, i.e., 8.8 cm. Before this location in the near field, the fluctuations of the SPL for the steered beam are smaller compared to that without the beam steering. This implies

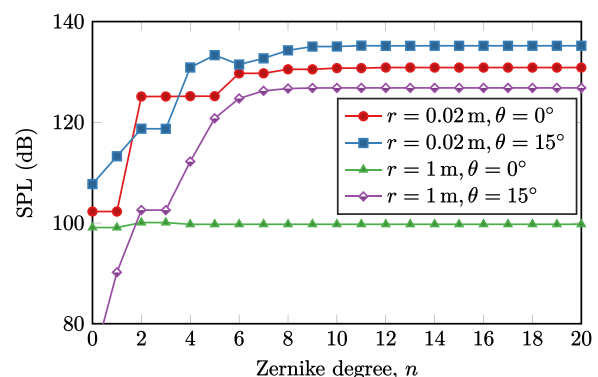


FIG. 4. (Color online) The ultrasound pressure level at several typical field points as a function of the truncation terms of Zernike degree n , where the ultrasound at 40 kHz is steered at the angle of $\phi_0 = 15^\circ$.

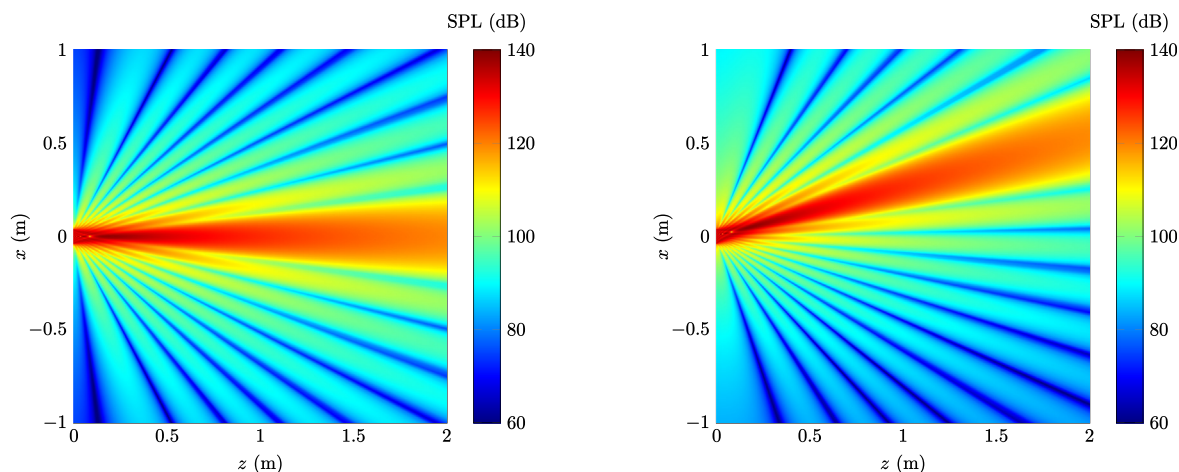


FIG. 5. (Color online) The ultrasound field at 40 kHz with the steering angle at (a) $\phi_0 = 0^\circ$ and (b) $\phi_0 = 15^\circ$, where the truncated degree of Zernike polynomials is 15. The dashed line denotes the beam direction.

that the major part of the energy of the steered beam remains at the same level when compared to that without the beam steering, so the generated audio sound in the main lobe would be similar.

C. Steerable PAL generating single beam

To examine the accuracy of the audio SPL when using Zernike polynomials to approximate the steering profile of the ultrasound, the audio SPL at several typical field points as a function of the truncated terms of the Zernike degree is presented in Fig. 7. It can be found the audio SPL at all field points converges at large Zernike degree n . The numerical results show the error is less than 0.1 dB for all points when the truncation terms are larger than 8. With the comparison of the convergence for ultrasound shown in Fig. 4, the required terms for the convergence of the audio sound are found to be slightly less than that of ultrasound.

Figure 8 shows the two-dimensional audio sound field at 1 kHz with and without the local effects, as well as the difference obtained with and without local effects. The radial audio SPL at the beam direction as a function of the radial distance is shown in Fig. 9. It is observed that the audio beam can be steered into the desired direction without

side lobes. The local effects make the SPL fluctuate in the near field for both cases, while the effects are negligible at large radial distances. It can be seen in Fig. 9 that the transition distance obtained by Eq. (12) can be used to determine if the local effects are significant. As the radial distance increases, starting from the transition distance at 0.19 m, the difference between the SPL obtained with and without the local effects decreases and finally converges to zero.

Figure 10 shows the two-dimensional audio sound field with the local effects at 250 Hz for a steering angle of 0° and 15° . Figure 11 compares the radial SPL at the beam direction with and without the local effects. It can be seen that a low audio frequency can also be steered to the desired direction without generating side lobes. The difference of the SPL obtained with and without the local effects is larger in the near field when compared to the case at 1 kHz, as shown in Fig. 9. For example, the SPL difference increases from 0.6 dB to 8.5 dB at the transition distance 0.19 m, with a steering angle of 15° when the frequency decreases from 1 kHz to 250 Hz. The reason is that the audio sound pressure determined by cumulative effects drops about 12 dB as the frequency is halved, while the Lagrangian density of ultrasound changes only a little, which results in significant local effects in the near field.¹³ However, it still holds that the

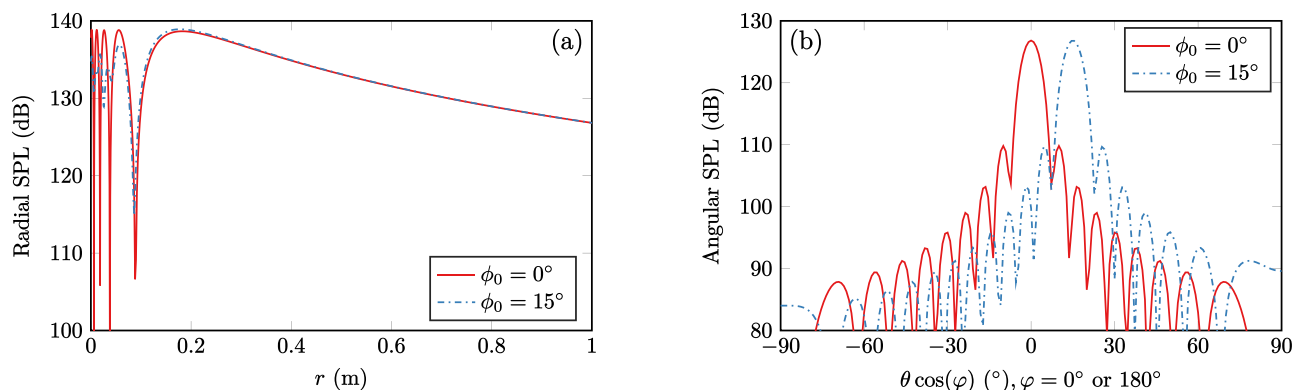


FIG. 6. (Color online) The ultrasound field at 40 kHz with the steering angle at 0° and 15° : (a) the radial SPL at the beam direction; (b) the angular SPL at a radial distance of 1 m.

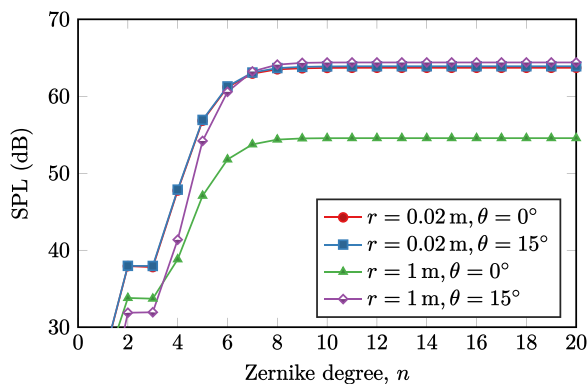


FIG. 7. (Color online) The audio SPL at several typical field points as a function of the truncated terms of Zernike degree n , where the audio sound at 1 kHz is steered at the angle of $\phi_0 = 15^\circ$.

difference decreases beyond the transition distance and eventually converges to zero.

D. Steerable PAL generating dual beams

Figure 12 shows the two-dimensional audio sound field when a steerable PAL generates dual beams at angles of 15° and -20° . Figure 13 presents the angular SPL at different radial distances as a function of the angle $\theta \cos \phi$, where $\phi = 0^\circ$ or 180° . All the results are given with the local effects. It can be found that the audio beams are successfully steered to dual directions and the main lobes are exactly at the angles of 15° and -20° . The results also show that the maxima obtained at two peaks at the beam directions are almost the same. It is noted in Fig. 13 that there is a local minimum near 0° . The differences between the maxima at two beam directions and the local minimum become smaller at smaller radial distances. For example, the difference

between the local maximum and minimum decreases from 7 to 4.4 dB as the radial distance decreases from 5 to 0.5 m. This implies that the two beams are not well separated at small radial distances in the near field. It also means that the prediction methods in the far field, e.g., the convolution model,⁶ underestimate the SPL at the location between two beam directions, which has also been demonstrated in Fig. 8 of Ref. 7. Nevertheless, all of the above numerical results demonstrate the proposed method is an accurate and efficient tool to predict and analyze both the near and far fields of the audio sound generated by a steerable PAL.

E. Computational efficiency

In this subsection, the computational efficiency is analyzed based on the numerical results obtained using a personal computer with an AMD Ryzen™ Threadripper™ 3960X (Santa Clara, CA) central processing unit (CPU) with 256 GB of random access memory (RAM). The audio sound pressure can be directly obtained by numerically evaluating the integral given by Eq. (9) (denoted by “direct method”), but it is too difficult to use in practice. First, the ultrasound pressure at large number of virtual source points \mathbf{r}_v needs to be calculated using Eq. (7), which is known to be very time-consuming due to the small ultrasonic wavelength compared to the aperture size, a . Second, the three-fold integral in Eq. (9) also requires heavy computations because the integration range is infinitely large in three dimensions. For example, it takes more than 1600 s to calculate the audio sound pressure at a single field point using the parameters in this paper. In addition, it is worth noting that the coordinates of field points, (x, y, z) , are coupled in the Green’s function in Eq. (9), which means the calculation

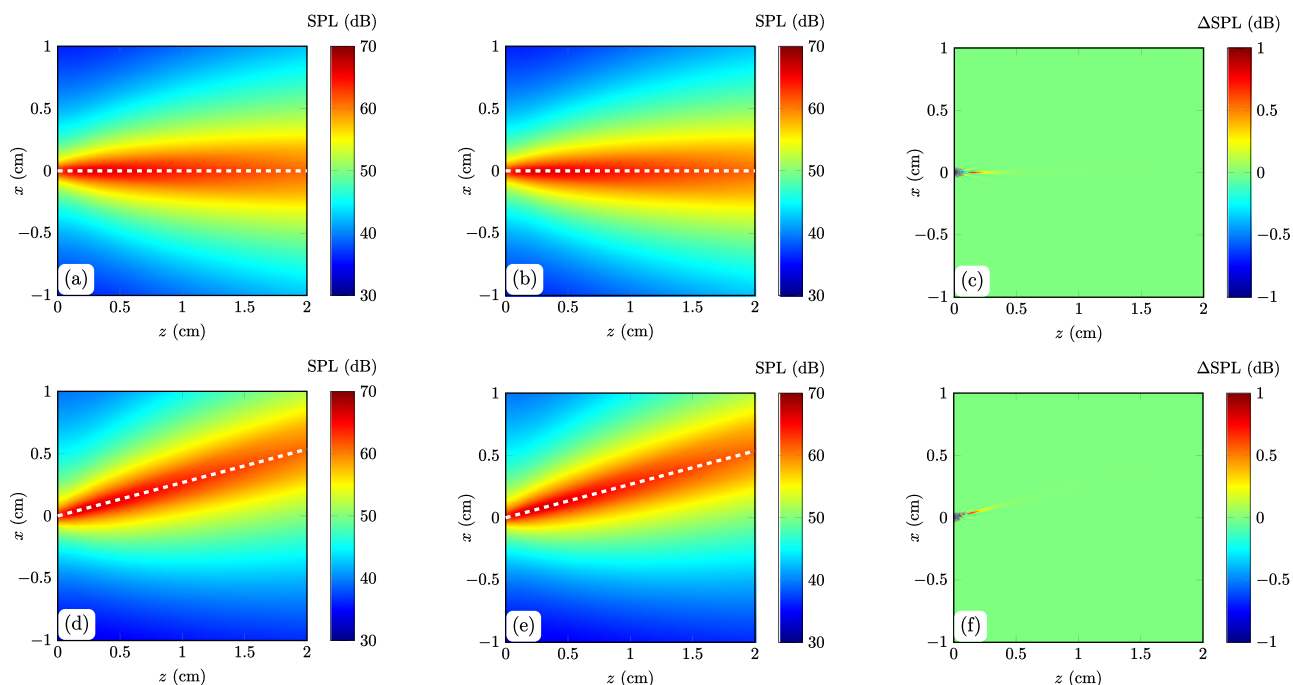


FIG. 8. (Color online) The audio sound field at 1 kHz with (left column) and without (middle column) the local effects, and the SPL difference (right column). Top row, the steering angle is $\phi_0 = 0^\circ$; bottom row, the steering angle is $\phi_0 = 15^\circ$. The dashed line denotes the beam direction.

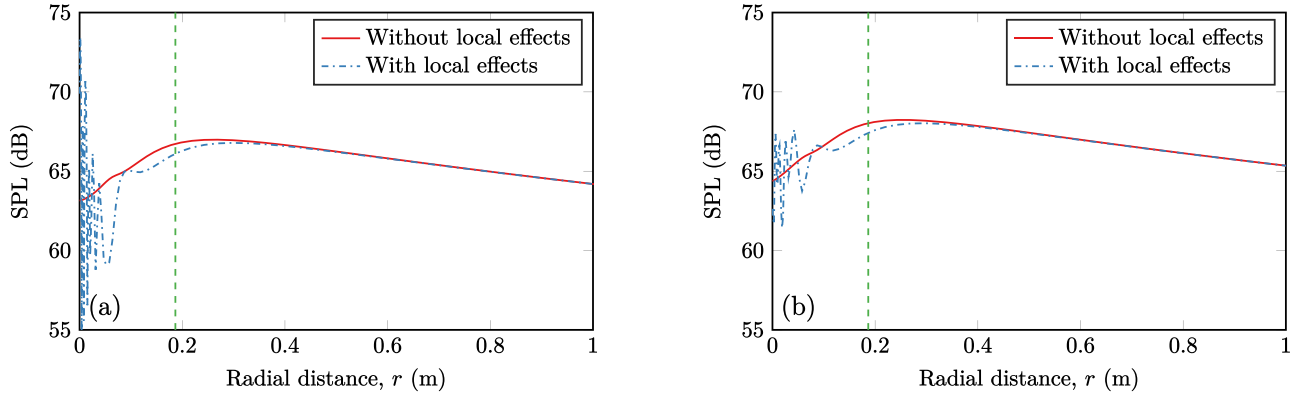


FIG. 9. (Color online) The audio SPL at the beam direction as a function of the radial distance with and without the local effects at 1 kHz: (a) the steering angle $\phi_0 = 0^\circ$; (b) the steering angle $\phi_0 = 15^\circ$. The dashed line denotes the transition distance at 0.19 m.

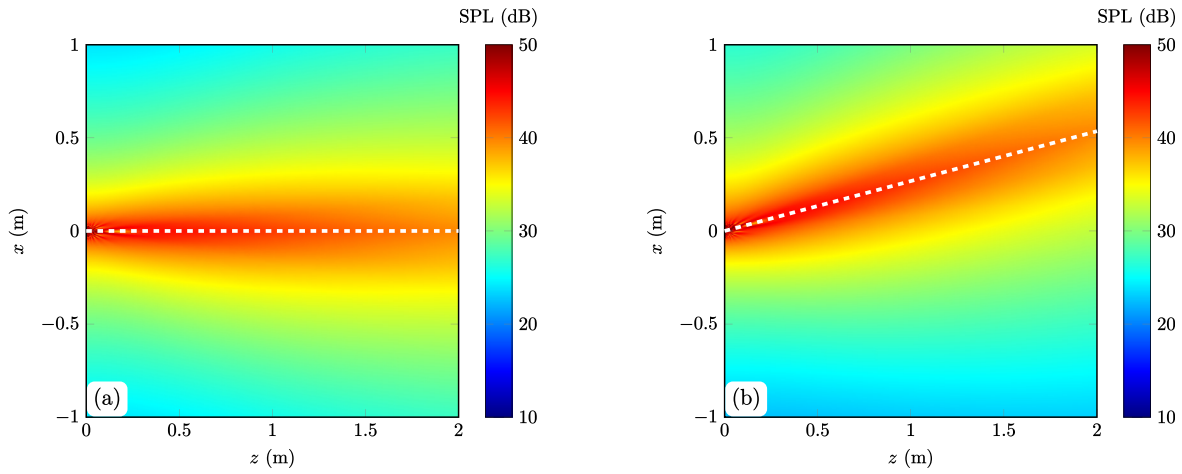


FIG. 10. (Color online) The audio sound field with the local effects at 250 Hz: (a) the steering angle is $\phi_0 = 0^\circ$; (b) the steering angle is $\phi_0 = 15^\circ$. The dashed line denotes the beam direction.

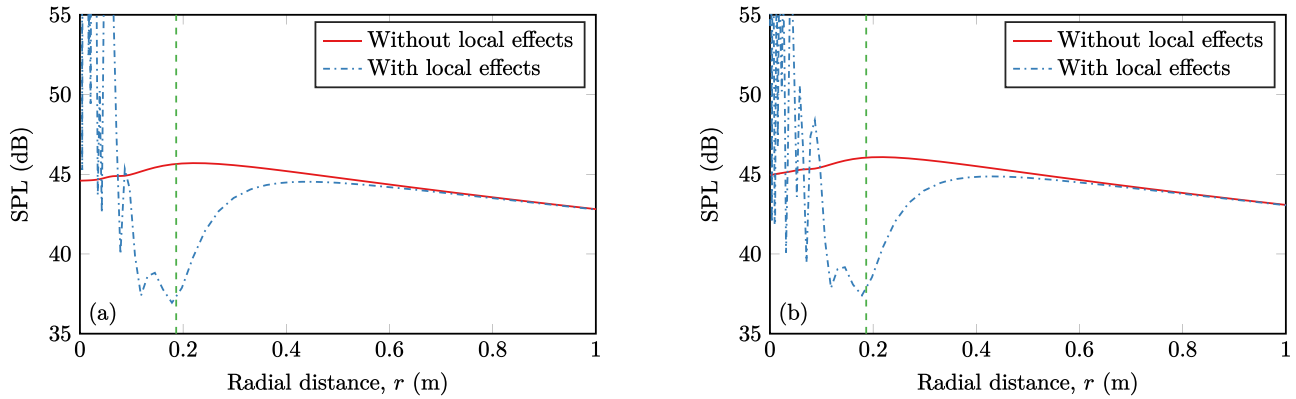


FIG. 11. (Color online) The audio sound field along the beam direction with and without the local effects at 250 Hz: (a) the steering angle is $\phi_0 = 0^\circ$; (b) the steering angle is $\phi_0 = 15^\circ$. The dashed line denotes the transition distance at 0.19 m.

time increases linearly as the number of the field points increases. Therefore, it is hard to obtain a two-dimensional sound field with many field points, such as Fig. 8.

For the proposed method, the audio sound pressure is calculated by adding the results contributed from all Zernike modes as shown by Eq. (36). For each Zernike mode, (\mathbf{n}, \mathbf{m}) , the audio sound is obtained using the SWE given by

Eq. (33), and it requires only around 1.2 s to obtain a converged result. As shown in Eqs. (13) and (36), the total number of truncated Zernike modes is $(N+2)^4/16$ and $(N+1)^2(N+3)^2/16$ when N is even and odd, respectively, where N is the truncated number for n_i . The required Zernike modes increases as the steering angle increases. For a special case when the steering angle $\phi_0 = 0^\circ$, $N=0$ as

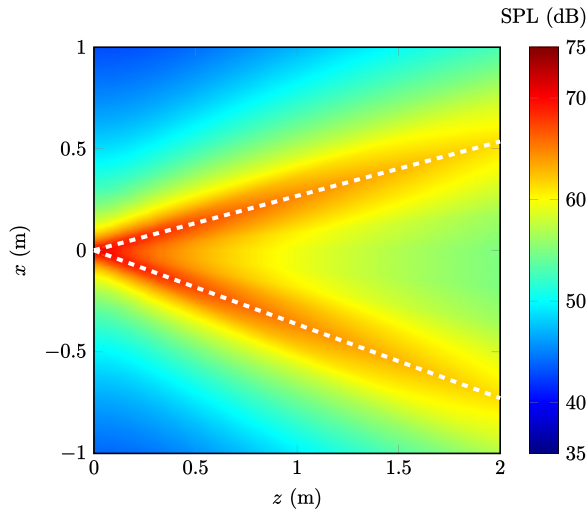


FIG. 12. (Color online) The audio sound field generated by a steerable PAL at 1 kHz generating dual beams at the angles of 15° and -20° . The dashed lines denote the beam directions.

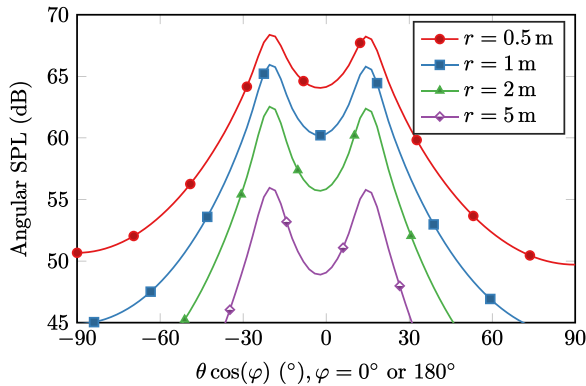


FIG. 13. (Color online) The angular audio SPL at different radial distances generated by a steerable PAL at 1 kHz generating dual beams at the angles of 15° and -20° .

demonstrated in Sec. III D. In this case, it takes only 1.2 s to obtained a converged result. For the investigated case in Sec. IV B when the steering angle $\phi_0 = 15^\circ$, $N=8$ and $(8+2)^4/16 = 625$ Zernike modes are required, so that it takes around 750 s to obtain the audio sound pressure at a single point which is less than half of the calculation time when using the direct method. Moreover, it is noted that the spherical coordinates of field points, (r, θ, φ) , are uncoupled in the proposed method shown in Eq. (33), which means the radial and angular components $[J_{\ell}^{n,m}(r) \text{ and } Y_{\ell}^{m-2\ell_3+|m-|}(\theta, \varphi)]$ can be calculated separately for a large number of field points. The numerical results show the elapsed time increases by about only 3 to 4 times when the field point number increases from 1 to 100, which is much more efficient than the direct method.

V. CONCLUSIONS

In this paper, Zernike circular polynomials are introduced to expand the velocity profile on the radiation surface of a steerable PAL. The closed-form expressions of the

expansion coefficients (Zernike moments) are derived. The existing computationally efficient SWE proposed in Refs. 12 and 13 is extended to calculate the radiation from a steerable using these Zernike polynomials. Compared to existing methods, the proposed expansion provides a rigorous transformation of the quasilinear solution of the Westervelt equation without additional approximations. The proposed expansion is further extended to accommodate the local effects by using an algebraic correction to Westervelt equation. The transition distance of whether the local effects are significant for a steerable PAL is investigated using the proposed method, and it is found to be the same as that for a conventional PAL. The numerical results obtained for single and dual beams demonstrate that the proposed method provides a useful tool to predict and analyze the sound field generated by a steerable PAL.

It is noted that the proposed SWE using Zernike polynomials provides a framework for the efficient and accurate calculation of audio sound fields generated by a PAL without additional paraxial approximations. Although the circular steerable PAL is investigated in this paper, the method is also applicable for any other excitation profiles, such as a focusing PAL. An arbitrary velocity profile on the radiation surface of the PAL can be expanded into a set of Zernike polynomials as shown by Eq. (13). The sound pressure generated by a PAL with Zernike profiles of all modes, $p_n^m(\mathbf{r})$, can be calculated first and saved as a table. The radiation from a PAL with an arbitrary profile can then be obtained by Eq. (36) after using this table and the Zernike moments. The radiation from a PAL which has other shapes instead of the circular shape can also be calculated using the proposed method. For example for a square PAL with a side length of $2a$, the square can be seen as a circle with a radius of $\sqrt{2}a$ and setting the velocity profile outside the square to zero.

ACKNOWLEDGMENTS

H.Z. gratefully acknowledges the financial support by National Natural Science Foundation of China (Grant No. 11874219).

¹W.-S. Gan, J. Yang, and T. Kamakura, "A review of parametric acoustic array in air," *Appl. Acoust.* **73**(12), 1211–1219 (2012).

²W.-S. Gan, J. Yang, K.-S. Tan, and M.-H. Er, "A digital beamsteerer for difference frequency in a parametric array," *IEEE Trans. Audio Speech Lang. Process.* **14**(3), 1018–1025 (2006).

³N. Tanaka and M. Tanaka, "Active noise control using a steerable parametric array loudspeaker," *J. Acoust. Soc. Am.* **127**(6), 3526–3537 (2010).

⁴C. Shi, Y. Kajikawa, and W.-S. Gan, "An overview of directivity control methods of the parametric array loudspeaker," *APSIPA Trans. Sign. Inf. Process.* **3**, 1–12 (2014).

⁵C. Shi, R. Bai, J. Gou, and J. Liang, "Multi-beam design method for a steerable parametric array loudspeaker," presented at the 2020 Asia-Pacific Signal and Information Processing Association Annual Summit and Conference (APSIPA ASC) (2020), pp. 416–420.

⁶C. Shi and Y. Kajikawa, "A convolution model for computing the far-field directivity of a parametric loudspeaker array," *J. Acoust. Soc. Am.* **137**(2), 777–784 (2015).

⁷J. Zhong, R. Kirby, M. Karimi, and H. Zou, "A cylindrical expansion of the audio sound for a steerable parametric array loudspeaker," *J. Acoust. Soc. Am.* **150**(5), 3797–3806 (2021).

- ⁸C. Shi and W.-S. Gan, "Product directivity models for parametric loudspeakers," *J. Acoust. Soc. Am.* **131**(3), 1938–1945 (2012).
- ⁹O. Guasch and P. Sánchez-Martín, "Far-field directivity of parametric loudspeaker arrays set on curved surfaces," *Appl. Math. Model.* **60**, 721–738 (2018).
- ¹⁰C. Shi, Y. Wang, H. Xiao, and H. Li, "Extended convolution model for computing the far-field directivity of an amplitude-modulated parametric loudspeaker," *J. Phys. D: Appl. Phys.* **55**(24), 244002 (2022).
- ¹¹M. Červenka and M. Bednařík, "Non-paraxial model for a parametric acoustic array," *J. Acoust. Soc. Am.* **134**(2), 933–938 (2013).
- ¹²J. Zhong, R. Kirby, and X. Qiu, "A spherical expansion for audio sounds generated by a circular parametric array loudspeaker," *J. Acoust. Soc. Am.* **147**(5), 3502–3510 (2020).
- ¹³J. Zhong, R. Kirby, and X. Qiu, "The near field, Westervelt far field, and inverse-law far field of the audio sound generated by parametric array loudspeakers," *J. Acoust. Soc. Am.* **149**(3), 1524–1535 (2021).
- ¹⁴J. Zhong, R. Kirby, M. Karimi, H. Zou, and X. Qiu, "Scattering by a rigid sphere of audio sound generated by a parametric array loudspeaker," *J. Acoust. Soc. Am.* **151**(3), 1615–1626 (2022).
- ¹⁵P. Ji and J. Yang, "An experimental investigation about parameters' effects on spurious sound in parametric loudspeaker," *Appl. Acoust.* **148**, 67–74 (2019).
- ¹⁶J. J. Wen and M. A. Breazeale, "A diffraction beam field expressed as the superposition of Gaussian beams," *J. Acoust. Soc. Am.* **83**(5), 1752–1756 (1988).
- ¹⁷M. Born and E. Wolf, *Principles of Optics*, 7th ed. (Cambridge University Press, Cambridge, 2019).
- ¹⁸R. Mukundan and K. Ramakrishnan, "Fast computation of Legendre and Zernike moments," *Pattern Recognit.* **28**(9), 1433–1442 (1995).
- ¹⁹R. M. Aarts and A. J. E. M. Janssen, "On-axis and far-field sound radiation from resilient flat and dome-shaped radiators," *J. Acoust. Soc. Am.* **125**(3), 1444–1455 (2009).
- ²⁰R. M. Aarts and A. J. Janssen, "Sound radiation quantities arising from a resilient circular radiator," *J. Acoust. Soc. Am.* **126**(4), 1776–1787 (2009).
- ²¹R. M. Aarts and A. J. E. M. Janssen, "Spatial impulse responses from a flexible baffled circular piston," *J. Acoust. Soc. Am.* **129**(5), 2952–2959 (2011).
- ²²R. M. Aarts and A. J. Janssen, "Sound radiation from a resilient spherical cap on a rigid sphere," *J. Acoust. Soc. Am.* **127**(4), 2262–2273 (2010).
- ²³W. P. Rdzanek, "The acoustic power of a vibrating clamped circular plate revisited in the wide low frequency range using expansion into the radial polynomials," *J. Acoust. Soc. Am.* **139**(6), 3199–3213 (2016).
- ²⁴W. P. Rdzanek, "Sound radiation of a vibrating elastically supported circular plate embedded into a flat screen revisited using the Zernike circle polynomials," *J. Sound Vib.* **434**, 92–125 (2018).
- ²⁵R. M. Aarts and A. J. E. M. Janssen, "Estimating the velocity profile and acoustical quantities of a harmonically vibrating loudspeaker membrane from on-axis pressure data," *J. Audio Eng. Soc.* **57**(12), 1004–1015 (2009), available at <https://www.aes.org/e-lib/browse.cfm?elib=15233>.
- ²⁶W. P. Rdzanek, "Sound scattering and transmission through a circular cylindrical aperture revisited using the radial polynomials," *J. Acoust. Soc. Am.* **143**(3), 1259–1282 (2018).
- ²⁷M. Červenka and M. Bednařík, "An algebraic correction for the Westervelt equation to account for the local nonlinear effects in parametric acoustic array," *J. Acoust. Soc. Am.* **151**(6), 4046–4052 (2022).
- ²⁸C. Shi, Y. Kajikawa, and W.-S. Gan, "Generating dual beams from a single steerable parametric loudspeaker," *Appl. Acoust.* **99**, 43–50 (2015).
- ²⁹M. Červenka and M. Bednařík, "A versatile computational approach for the numerical modelling of parametric acoustic array," *J. Acoust. Soc. Am.* **146**(4), 2163–2169 (2019).
- ³⁰S. I. Aanonsen, T. Barkve, J. N. Tjøtta, and S. Tjøtta, "Distortion and harmonic generation in the nearfield of a finite amplitude sound beam," *J. Acoust. Soc. Am.* **75**(3), 749–768 (1984).
- ³¹Y. Kagawa, T. Tsuchiya, T. Yamabuchi, H. Kawabe, and T. Fujii, "Finite element simulation of non-linear sound wave propagation," *J. Sound Vib.* **154**(1), 125–145 (1992).
- ³²C.-W. Chong, P. Raveendran, and R. Mukundan, "A comparative analysis of algorithms for fast computation of Zernike moments," *Pattern Recognit.* **36**(3), 731–742 (2003).
- ³³M. Abramowitz and I. A. Stegun, *Handbook of Mathematical Functions with Formulas, Graphs and Mathematical Tables* (National Bureau of Standards, Washington, DC, 1972).
- ³⁴B. Rafaely, *Fundamentals of spherical array processing*, in *Springer Topics in Signal Processing* (Springer, Berlin, 2015), Vol. 8.
- ³⁵S. Zhang and J. Jin, *Computation of Special Functions* (Wiley, New York, 1996).
- ³⁶P. A. Martin, *Multiple Scattering: Interaction of Time-harmonic Waves with N Obstacles*, Encyclopedia of Mathematics and its Applications (Cambridge University Press, Cambridge, 2006).
- ³⁷A. Messiah, *Quantum Mechanics: Volume II* (North-Holland, Amsterdam, 1962).